Available online at www.sciencedirect.com
SCIENCE DIRECT®
ELSEVIER
Physica D 187 (2004) 338–357
PHYSICA D
www.elsevier.com/locate/physd

Lyapunov spectra and nonequilibrium ensembles equivalence in 2D fluid mechanics

Giovanni Gallavotti [a], Lamberto Rondoni [b,*], Enrico Segre [c]

[a] *Fisica, Università di Roma "La Sapienza", P.le Moro 2, I-00185 Rome, Italy*
[b] *DIMAT and INFM, Politecnico di Torino, Corso Duca degli Abruzzi 24, I-10129, Turin, Italy*
[c] *DIASP, Politecnico di Torino, Corso Duca degli Abruzzi 24, I-10129 Turin, Italy*

Abstract

We perform numerical experiments to study the Lyapunov spectra of dynamical systems associated with the Navier–Stokes (NS) equation in two spatial dimensions truncated over the Fourier basis. Recently new equations, called GNS equations, have been introduced and conjectured to be equivalent to the NS equations at large Reynolds numbers. The Lyapunov spectra of the NS and of the corresponding GNS systems overlap, adding evidence in favor of the conjectured equivalence already studied and partially extended in previous papers. We make use of the Lyapunov spectra to study a fluctuation relation which had been proposed to extend the "fluctuation theorem" to strongly dissipative systems. Preliminary results towards the formulation of a local version of the fluctuation formula are also presented.

PACS: 05.70.Ln; 47.27.Ak; 65.50.+m

Keywords: Local and global fluctuation relations; Axiom C; Entropy production; Turbulence

1. Introduction

The idea of viewing turbulent fluid motions as trajectories in the phase space of a chaotic dynamical system is a long standing one. In particular, treating turbulence in terms of invariant probability distributions on the phase space of the dynamical system given by the Navier–Stokes (NS) equation for a fluid, and asserting that the distributions ought to have special properties, is an idea which dates back to the early 1960s: it has been formalized a little later, see [1].[1]

Mathematical and numerical studies have been performed, at first for the purpose of relating fluid dynamical parameters, such as the Reynolds number or the amplitude of external forcing, to the fractal dimension of the

* Corresponding author.
E-mail addresses: gallavotti@roma1.infn.it (G. Gallavotti), rondoni@polito.it (L. Rondoni), segre@athena.polito.it (E. Segre).

[1] Quoting [2], "It is widely accepted that the statistical properties of a turbulent flow can be described by a dynamical evolution on a strange attractor in a high-dimensional phase space. An important characterization of the ergodic properties of the attractor is given by the Lyapunov spectrum."

0167-2789/$ – see front matter © 2003 Elsevier B.V. All rights reserved.
doi:10.1016/j.physd.2003.09.029

attractor.[2] In this way, the onset of turbulence has been quite well understood, along with the discovery that the relevant physical phenomena are far more interesting and complex than previously anticipated, see [3–7].

However, understanding developed turbulence remains a most challenging problem and it is not clear how to use the basic ideas of Lorenz, Ruelle and Takens in this context. The approach to the analysis is very often based on numerical experiments in which simulations of reduced models of turbulence are considered. For instance, the shell models of Yamada and Okhitani [8,9], and Benzi et al. [10] have been studied in great detail with the aim of finding or checking connections between Lyapunov spectra and the turbulent cascade.

Another viewpoint [11,12] stems from the well-known fact that macroscopic irreversibility of particle systems can be obtained from microscopic reversible dynamics, provided the ratios between the microscopic and the macroscopic time and length scales are sufficiently large. In that case, in fact, the microscopic reversible equations of motion are "equivalent" to dissipative equations of motion at the macroscopic level.

Assuming that forced turbulence is described by the (irreversible) NS equation, a different (reversible) equation called the "Gaussian–Navier–Stokes", or GNS, equation was proposed to describe the same physical phenomena [11,12]. In the GNS equation the usual viscosity constant is replaced by a fluctuating term, which makes the equation itself *time reversal invariant* and keeps the total energy exactly constant. Equivalence should occur when the constant energy of the GNS evolution equals the average energy in the NS evolution provided the Reynolds number is large: in a way which is similar to the equivalence between microcanonical and canonical ensembles in statistical mechanics [13], with the large volume limit replaced by the limit of large Reynolds number R. The conjecture states that the forward time statistics of the NS and of the GNS models of the same fluid are the same, for what concerns "local observables", i.e. for the time averages of functions of the velocity field which depend only on a small number of its Fourier components physically corresponding to observables on the inertial scale.

The idea, if correct, could be used to analyze phenomena which would not be easily understood in terms of the NS equation. For instance, time reversal invariance and chaoticity of the GNS dynamics imply that the fluctuations of certain quantities obey a relation (cf. [14]), here referred to as "fluctuation relation" (FR), which might eventually be amenable to experimental tests as attempted in [15,16].[3] It should be remarked that the possibility of using several different representations of the statistical properties of a turbulent fluid flow, which result equivalent from a practical point of view, was considered already in previous works, see, e.g. [19–21], and is still under investigation [22].

Of course, despite the expected equivalence, the NS and GNS representations of a turbulent fluid remain different, similarly to the microcanonical and the canonical ensembles descriptions of equilibrium statistical mechanics: although "equivalent in the thermodynamic limit" they differ in many respects (e.g. in the distribution of fluctuations of the total energy).

[2] It is important, when discussing fractality, to distinguish between *attractor* and *attracting set*. An attracting set is a *closed set* such that all points in its vicinity get as close as one wants to the set as time tends to infinity and, *furthermore*, such that none of its closed subsets have the same property. The notion of attractor is associated with a method of choice of initial data in the vicinity of an attracting set. Suppose that the data are randomly selected with a distribution μ_0 and, with μ_0 − probability 1, their asymptotic motion is described by a probability distribution μ on the attracting set, in the sense that time averages can be obtained simply by integration with respect to μ. Then, *any* subset of the attracting set with μ_0 − probability 1 *and* smallest Hausdorff dimension is called "*attractor*" for the random choices with distribution μ_0, and μ is called the *statistics* of μ_0. Quite commonly, the attracting set is not fractal, and it might even coincide with the whole phase space, while the attractor for (some) μ_0 is fractal and with dimension lower than that of the attracting set. We recall that the special statistics generated on an attracting set from data randomly chosen with a probability distribution μ_0 absolutely continuous with respect to the volume is called a "*SRB distribution*", which is usually unique: in this paper we shall, as usual, only consider the SRB statistics.

[3] It is important to note that there are several fluctuation relations which look similar to the FR we consider in this paper. These relations are interesting of their own merits, but will not be considered here because they are not related to the FR. For instance, the Transient Fluctuation Formula (TFF) derived by Evans and Searles in [17] concerns non-stationary probability distributions, while the FR refers to the SRB distribution, i.e. to the statistics of the motion (cf. [18] for a discussion of the differences between the FR and the TFF).

2. NS and GNS equations: aims of our analysis

Suppose that the side of the periodic cell is L, and that the forcing term $\boldsymbol{f}$ is the product of a dimensional parameter F times a fixed function. We shall suppose the Fourier components $F_{\boldsymbol{k}}$ to have modulus 1 and, usually, to vanish for all but one value of $\boldsymbol{k}$.[4] Then, in the NS case with viscosity ν, we define the *Reynolds number* R to be

$$R^2 = FL^3\nu^{-2}, \quad \text{or} \quad R = \nu^{-1}\sqrt{FL^3}. \tag{1}$$

and we shall consider the NS equations in dimensionless form. Here, the lengths are measured in units of $L^2/2\pi$ and time in units of L^2/ν, so that the change of variables $\boldsymbol{u}(x,t) = V\boldsymbol{u}^g(\boldsymbol{x}/L, Ct)$ with $V = FL^2/\nu$, $C = \nu/L^2$, yields (redefining simply by $\boldsymbol{u}$ the dimensionless field $\boldsymbol{u}^g$ for notational convenience) the *dimensionless NS equations*

$$\dot{\boldsymbol{u}} + R^2(\boldsymbol{u}\cdot\partial)\boldsymbol{u} = \Delta\boldsymbol{u} + \boldsymbol{f} - \partial p, \quad \partial\boldsymbol{u} = 0 \tag{2}$$

with $\boldsymbol{u}$ periodic in the position coordinates with period 2π and *divergenceless* (i.e. $\boldsymbol{u}$ represents an incompressible flow). Correspondingly, the GNS equations will be defined by

$$\dot{\boldsymbol{u}} + R^2(\boldsymbol{u}\cdot\partial)\boldsymbol{u} = \alpha\Delta\boldsymbol{u} + \boldsymbol{f} - \partial p, \quad \partial\boldsymbol{u} = 0 \tag{3}$$

where R is a free parameter and α is defined so that the solutions of the Eq. (3) conserve $Q_0 = \int \boldsymbol{u}^2\,\mathrm{d}\boldsymbol{x}$, i.e. twice the total kinetic energy.

In order to compare motions that the GNS equations generate with (suitably selected) motions of the NS fluid, the constant Q_0 has to be chosen. For a given R and taking as reference the NS equation, we call $\langle Q_0\rangle$ the infinite time average of Q_0 produced by the NS evolution. We shall compare, according to the analysis of [23,24], the solutions of the NS equation with those of the GNS equations with the conserved quantity Q_0 set equal to $\langle Q_0\rangle$.

We write $\boldsymbol{u}(\boldsymbol{x}) = \sum_k \mathrm{e}^{\mathrm{i}\boldsymbol{k}\cdot\boldsymbol{x}}u_{\boldsymbol{k}}\boldsymbol{k}^\perp/|\boldsymbol{k}|$, where the scalar term $u_{\boldsymbol{k}}$ obeys $u_{\boldsymbol{k}} = -\bar{u}_{-\boldsymbol{k}}$, and $\boldsymbol{k}^\perp = (k_2, -k_1)$ if $\boldsymbol{k} = (k_1, k_2)$. Hence, $Q_0 = (2\pi)^2\sum_{\boldsymbol{k}}|u_{\boldsymbol{k}}|^2$ (and the total vorticity is $Q_1 = (2\pi)^2\sum_{\boldsymbol{k}}|\boldsymbol{k}|^2|u_{\boldsymbol{k}}|^2$). If we define the effort $\boldsymbol{G}_1$ as

$$\begin{aligned}\boldsymbol{G}_1 &= (\Delta^{-1}(\boldsymbol{a} - \boldsymbol{f} - \partial p), (\boldsymbol{a} - \boldsymbol{f} - \partial p))\\ &= (2\pi)^2\sum_{\boldsymbol{k}}\frac{1}{\boldsymbol{k}^2}\left(\dot{u}_{\boldsymbol{k}} + \mathrm{i}R^2\sum_{\boldsymbol{j}+\boldsymbol{h}=\boldsymbol{k}}((\boldsymbol{j}^\perp\cdot\boldsymbol{h})(\boldsymbol{h}\cdot\boldsymbol{k})/|\boldsymbol{j}|\boldsymbol{h}|\boldsymbol{k}|)u_{\boldsymbol{j}}u_{\boldsymbol{h}} - f_{\boldsymbol{k}}\right)^2\end{aligned} \tag{4}$$

where $(\cdot,\cdot)$ denotes the usual scalar product in $L_2(\mathrm{d}\boldsymbol{x})$, and $a = \mathrm{d}\boldsymbol{u}/\mathrm{d}t = \partial_t\boldsymbol{u} + R^2(\boldsymbol{u}\cdot\partial)\boldsymbol{u}$ is the acceleration field, Eq. (3) can be obtained from Gauss' least effort principle by considering an Euler fluid subject to the constraint of constant Q_0, i.e. constant total energy. In this case the acceleration $\boldsymbol{a}$ of the velocity field $\boldsymbol{u}$ minimizes the effort $\boldsymbol{G}_1$ among all possible accelerations compatible with the incompressibility and with the constraint. If we write Eq. (3) in terms of Fourier components we find

$$\dot{u}_{\boldsymbol{k}} = -\mathrm{i}R^2\sum_{\boldsymbol{j}+\boldsymbol{h}=\boldsymbol{k}}\frac{(\boldsymbol{j}^\perp\cdot\boldsymbol{h})(\boldsymbol{h}\cdot\boldsymbol{k})}{|\boldsymbol{j}|\boldsymbol{h}|\boldsymbol{k}|}u_{\boldsymbol{j}}u_{\boldsymbol{h}} - \alpha\boldsymbol{k}^2u_{\boldsymbol{k}} + f_{\boldsymbol{k}} \tag{5}$$

where α is given by

$$\alpha = \frac{\sum_{\boldsymbol{k}} f_{\boldsymbol{k}}\bar{u}_{\boldsymbol{k}}}{\sum_{\boldsymbol{k}}|\boldsymbol{k}|^2|u_{\boldsymbol{k}}|^2}. \tag{6}$$

[4] The cases of Fig. 2 are the only exceptions considered here.

Of course the fact that the equations above can be obtained from a variational principle might be merely accidental, and in itself does not justify their use. However, in [11,12,23,24] it has been argued that they should give a description of the fluid motions which in the large Reynolds number regime is as accurate as the NS equations themselves. More generally, one can consider an Euler fluid subject to a Gaussian constraint on Q_m with effort function G_ℓ $\ell \le m+1$, given by

$$Q_m = (2\pi)^2 \sum_{\boldsymbol{k}} |\boldsymbol{k}|^{2m} |u_{\boldsymbol{k}}|^2, \qquad \boldsymbol{G}_{\ell,m} = ((\Delta)^{-(\ell-m)}(\boldsymbol{a} - \boldsymbol{f} - \partial p),\ (\boldsymbol{a} - \boldsymbol{f} - \partial p)). \tag{7}$$

This leads to equations like (3) with the Laplace operator replaced by Δ^ℓ, and with α replaced by a new coefficient $\beta_{\ell,m}$ that can be easily computed by imposing that Q_m remains exactly constant. We call the resulting equations "G-*hyperviscous*" equations while we call "*hyperviscous*" the corresponding equations in which $\beta_{\ell,m}$ is replaced by a constant. The above case (5) corresponds to $\ell = 1, m = 0$. The special cases $\ell = 0, m = 0$ and $\ell = 1, m = 1$ have been considered in [11] and the general hierarchy of the hyperviscous equations has been considered and partially studied in [24]. The case $\ell = 1, m = 1$, for instance, yields

$$\beta_{1,1} = \frac{\sum_{\boldsymbol{k}} |\boldsymbol{k}|^2 f_{\boldsymbol{k}} \bar{u}_{\boldsymbol{k}}}{\sum_{\boldsymbol{k}} |\boldsymbol{k}|^4 |u_{\boldsymbol{k}}|^2}. \tag{8}$$

A general feature of the G-hyperviscous equations is that they generate *reversible dynamics* in the sense that the velocity reversal operation $Iu_{\boldsymbol{k}} = -u_{\boldsymbol{k}}$ anticommutes with the time evolution map S_t (the mapping of an initial datum $\boldsymbol{u}$ into its value $S_t\boldsymbol{u}$ at time t) in the sense that

$$I \cdot S_t = S_{-t} \cdot I. \tag{9}$$

Note that here we call GNS equations the case $\ell = 1, m = 0$ for consistency with [24] because we shall often refer to [24], although in [11] this name was used for the case $\ell = 1, m = 1$.

In this paper, we study the following via computer simulations:

(1) *Relations between the Lyapunov spectra of corresponding NS and GNS models:* Equivalence between the Lyapunov spectra is not part of the earlier proposals on equivalence because the Lyapunov exponents are not "local observables": however it seems possible that they reflect properties of the individual modes of the velocity field [25] so that it is interesting to test whether equivalence extends to them. In the models that we consider the Lyapunov spectra appear to be essentially *identical* within the errors.

(2) *Fluctuation properties:* Fluctuation properties of the observable defined by the phase space contraction in the reversible GNS equation and its relation with the Lyapunov spectra following the proposal in [11]. The relation proposed in [11] is, however, based on several assumptions which we cannot check directly. Therefore, we have measured quantities for which predictions are available as consequences of the mentioned assumptions, finding that the predictions match with the observations. This lends support to the idea that the property called "*axiom C*" as well as the assumptions on the structure of the attracting sets discussed in [11,26] may actually belong to the models considered here.

(3) *Equivalence analysis:* The equivalence analysis can be extended to involve not only NS and GNS equations but also to several members of the hierarchy of hyperviscous and G-hyperviscous equations. We have made a few tests analogous to those made in the case of the NS and GNS equations, and some of the results are briefly presented below.

(4) *Local fluctuations:* The theory of the fluctuations of α considered in item (2) above concerns the global phase space contraction rate, which in our models is extensive. Extensivity makes it very difficult to measure the fluctuations of α in systems with a large number of modes (i.e. many degrees of freedom). To overcome this

difficulty, we define and study the "local phase space contraction" related to a portion of the volume occupied by the fluid, where fluctuations are strongly enhanced.

The investigation is important because in comparing fluctuations of phase space contraction between corresponding NS and GNS evolutions one must look at smaller subsystems. For instance, in the (truncated) NS equation there is no fluctuation of the total phase space contraction rate, because the friction coefficient is constant: the phase space contraction rate (i.e. the divergence of the equations of motion) is simply $-2\sum_{|\boldsymbol{k}|<N} \boldsymbol{k}^2$ if N is the cut off parameter (the summation runs over the independent modes).

Furthermore, in real experiments, one is forced to look at the fluctuations within small portions of fluid in order to obtain good statistics [15,16]. Our results on this matter are only preliminary, but encouraging, so we report them in Appendix A.

We integrated Eq. (5) by means of a pseudospectral code truncating it to a small number K of Fourier modes, $u_{\boldsymbol{k}}$, of the velocity field. The computation of the entire Lyapunov spectrum is, generally, expensive (in terms of CPU time), and testing the validity of the FR (for the GNS equation) requires high statistics on the fluctuations of the phase space contraction rate α. Thus we have been forced to adopt a "low resolution" approximation of the dynamics in Fourier space: i.e. to take $\boldsymbol{k}, \boldsymbol{p}, \boldsymbol{q} \in [-(N-1), \ldots, (N-1)]^2$, where N is a small truncation value. In this way, the number of independent real components of the velocity field is $2K$ with $2K = 4N(N-1)$ not counting the components corresponding to $\boldsymbol{k} = \boldsymbol{0}$ which, being constants of motion, have been fixed to be zero. We say that the equations are "truncated at K modes" calling "mode $\boldsymbol{k}$" a (complex) Fourier component $u_{\boldsymbol{k}}$ of the velocity field. In our cases $2K$ ranges between 24 and 168: this corresponds to $N-1$ between 2 and 6. Given our Reynolds numbers, K is much less than the value it should have (which we estimate to be about one order of magnitude higher) in order to interpret the results as relevant for developed turbulence (albeit in two dimensions), consistently with the theories of homogeneous turbulence. However, our present computer facilities make it impossible for us to reach much higher numbers of modes with the precision demanded by our analysis.

3. Extension of equivalence between the NS and GNS dynamics to Lyapunov spectra

The equivalence principle introduced in [11,23] yields quantitative relations between certain observables, which can be tested in numerical experiments. The principle states that NS and GNS equations should have same statistics for the "local observables",[5] when the limit of large Reynolds number is taken and the average phase space contraction of the GNS evolution equals the (constant) phase space contraction rate of the NS evolution.

The phase space contraction rate associated with a differential equation is the divergence of the equations of motion: it can be straightforwardly computed from Eqs. (5) and (6) to be $\sigma = (-1 + 2\sum_{|k_i|<N} 1) \cdot \alpha$ in the case $\ell = 0$ and $m = 0$ (which we call GED case), and

$$\sigma^{\mathrm{GNS}} = 2\left(\sum_i |k_i|^2 - \frac{Q_2}{Q_1}\right) \cdot \alpha + \frac{\sum_{|k|<N} \boldsymbol{k}^2 f_{k_i} \bar{u}_{k_i}}{Q_1} \tag{10}$$

in the GNS case, i.e. for $\ell = 1$, $m = 0$ (see Eq. (7)).[6] Denoting by

$$\sigma^{\mathrm{NS}} = 2 \sum_{|k_i|<N} |k_i|^2 = M \tag{11}$$

[5] That is, for the time averages of functions of the velocity field which depend only on a finite number of its Fourier components or, more generally and more physically, which depend only on Fourier components of modes with k in the inertial range.

[6] In experiments on real fluids this quantity must be associated with some physical observable (a very delicate matter [15,16]).

the (constant) phase space contraction rate of the NS evolution, and by

$$\langle \sigma^{\mathrm{GNS}} \rangle = \left\langle 2 \left(\sum_i |k_i|^2 - \frac{Q_2}{Q_1} \right) \cdot \alpha + \frac{\sum_{|k_i|<N} \boldsymbol{k}^2 f_i \bar{u}_{k_i}}{Q_1} \right\rangle = M \cdot \langle \alpha \rangle + \mathrm{o}(M) \tag{12}$$

the average phase space contraction rate of the GNS evolution, the equivalence conjecture studied in [24] can be stated as follows.

Equivalence Conjecture (EC). *The stationary probability distributions on the phase space associated with the NS equations and the GNS equations are equivalent in the limit of large Reynolds number, provided the value of Q_0 is chosen so that σ^{NS} and $\langle \sigma^{GNS} \rangle$ coincide or, equivalently, provided the value of Q_0 is chosen so that $\langle \alpha \rangle$ equals* 1.[7]

The idea behind this conjecture is that if the fluctuations of α occur on time scales which are short compared with the macroscopic observation time scales, and if $\langle \alpha \rangle = 1$, the macroscopic observables should be equally well computed from the NS and the GNS dynamics. The large R limit is, then, required to ensure that the fluctuations of α do really occur on sufficiently short time scales. The results of [24] suggest that this is the case.

To obtain such results, the steady state of the NS evolution was first determined by following, during a long time T, the approach of the time average of Q_0 to its asymptotic value $\langle Q_0 \rangle$ At time T, the evolution was continued with the GNS dynamics with initial condition taken to be the vorticity field produced by the NS dynamics at time T. It was then observed that $\langle \sigma^{\mathrm{GNS}} \rangle / \sigma^{\mathrm{NS}} \approx \langle \alpha \rangle$ and that $\langle \alpha \rangle$ differ little from 1 already at small N (of order $\mathrm{O}(10^1)$ and even less) *as long as the initial* (*fixed*) *value* Q_0^{GNS} *of* Q_0 *was close to its NS time average* $\langle Q_0 \rangle$. Furthermore the details of the initial condition for the GNS evolution did not affect *too much* the statistical results produced by the GNS dynamics. In other words, it appeared that only the parameter Q_0^{GNS} needs to be adjusted to obtain equivalent NS and GNS evolutions. Although the meaning of "*too much*" and "*close*" was not sharply quantified in [24], the results suggested the validity of an EC also in the following alternative sense:

Equivalence Conjecture (EC′). *The stationary phase space probability distributions of the NS equations and of the GNS equations are equivalent in the limit of large Reynolds number, provided the energy Q_0 is fixed in the GNS evolution to coincide with the average value $\langle Q_0 \rangle$ of the NS evolution at the same* (*large*) R.

In this paper, we first investigate the possibility of extending the EC and EC′ to the equivalence of the Lyapunov spectra. We evaluate the Lyapunov exponents of the NS equation by performing a long numerical simulation from time 0 up to time T, yielding the NS Lyapunov spectrum and the average value $\langle Q_0 \rangle$, with an error bar δQ_0. From time T, we continue the NS evolution until Q_0, which fluctuates, equals $\langle Q_0 \rangle$. This usually takes a short time t_{s}. Then, at time $T + t_s$, we switch to the GNS evolution and compute the corresponding GNS Lyapunov spectrum. The reason ion adopting this procedure, rather than just taking a random initial field with $Q_0^{\mathrm{GNS}} = \langle Q_0 \rangle$ for the GNS evolution, is that, a priori, the attractor might be not unique, and different initial fields may be evolved by the GNS dynamics towards attractors different from the one found by following the NS evolution. In other words, the NS and the GNS statistical properties may not always result comparable because of possible hysteresis phenomena. Our procedure was originally designed to avoid this problem, although it turned out subsequently that our choice of parameters yields no hysteresis, as discussed in [27].

The Lyapunov spectra produced by the NS and GNS dynamics in this way appear *equivalent*, meaning that the Lyapunov spectra of the NS and GNS dynamics appear to become identical for large R and K. At finite R and K,

[7] Equals the viscosity in our dimensionless units.

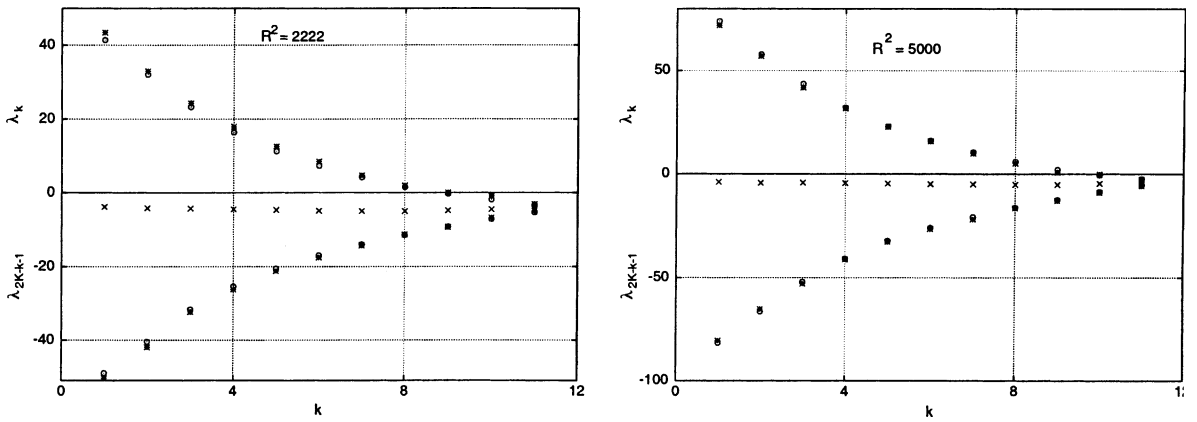

Fig. 1. Lyapunov spectra for the NS runs with normal viscosity ($\ell = 1$) at $R^2 = 2222$ (left) and $R^2 = 5000$ (right), and corresponding GNS runs with constrained energy Q_0. The forced modes are (0,±2). The $2K - 2$ nontrivial exponents are drawn by associating each value of the abscissa $k = 1, 2, \ldots, K-1$ with the kth largest exponent λ_k and the kth smallest exponent $\lambda'_k = \lambda_{2K-k-1}$. The symbols "$\odot$" refer to the NS spectra, the "$*$" to the GNS spectra, and the "$\times$" to the sums $(\lambda_k + \lambda'_k)/2$ for the NS case. There is no "pairing" of the exponents to a common average value, unlike the cases of isokinetic Gaussian systems [29]. Essentially identical results have been obtained by studying the ED and GED equations.

instead, the sums of the Lyapunov exponents should be related by (cf. Eqs. (11) and (12))

$$\sum_{i=1}^{k} \lambda_i^{\mathrm{GNS}} = \sum_{i=1}^{k} \lambda_i^{\mathrm{NS}} + \mathrm{o}(M), \quad \text{where} \quad \sum_{i=1}^{k} \lambda_i^{\mathrm{NS}} = -M. \tag{13}$$

The typical situation is represented in Fig. 1 where the $2K - 2$ nontrivial exponents are drawn. Note that two exponents are a priori known to vanish in the GNS case: one corresponding to the direction of motion and one to the direction of the conserved quantity; in the NS case one is a priori known to vanish, corresponding to the direction of motion. However, in all cases the NS evolution shows another exponent very close to zero in agreement with the equivalence conjecture and we have taken it to be zero in drawing the Figs. 1 and 2 (see also footnote 11).

The Lyapunov exponents are obtained by the method of [28] over times T of the order of up to 10^5 Lyapunov time units.[8] Error bars do not appear, since they are not larger than the size of the symbols in the figures, as explained in Section 5.

Consistent with the EC′, and up to numerical errors, we observed that the viscosities and the average enstrophies of the NS and GNS evolutions with $2K = 24$ give equal results if the average energies are equal. The numerical errors we refer to can be attributed to our approximate knowledge of the average of Q_0 (which is affected by an error bar δQ_0); and to the finite values of R, N, and T (which, in turn, can only be reached through a sequence of time steps of finite size h). The corresponding deviations from the conjectured equalities of the viscosities and of the average enstrophies are measured by the terms $\Delta\alpha = (\langle\alpha\rangle - 1)$ and $\Delta Q_1 = |\langle Q_1\rangle_{\mathrm{NS}} - \langle Q_1\rangle_{\mathrm{GNS}}|/\langle Q_1\rangle_{\mathrm{NS}}$ in Tables 1 and 2, where the subscripts NS and GNS indicate the two relevant kinds of dynamics.

Further computations of the Lyapunov spectra were performed for $2K = 168$, starting from random initial data, evolving with the NS evolution, and then switching to a GNS evolution, as above. In this case, however, the fixed quantity Q_m of the GNS evolution was the energy Q_0 in one instance, the enstrophy Q_1 in another instance, and the palinstrophy Q_2 in the last instance. The motivation behind this computation was to check the validity of the conjecture, proposed and partially tested in [24], that "several" pairs of equations of the hierarchies of hyperviscous and G-hyperviscous equations with $\ell \le m + 1$, are equivalent to each other in the limit of large Reynolds numbers.

[8] We define the Lyapunov time unit as $1/\lambda_{\max}$, where $\lambda_{\max}$ is the largest Lyapunov exponent.

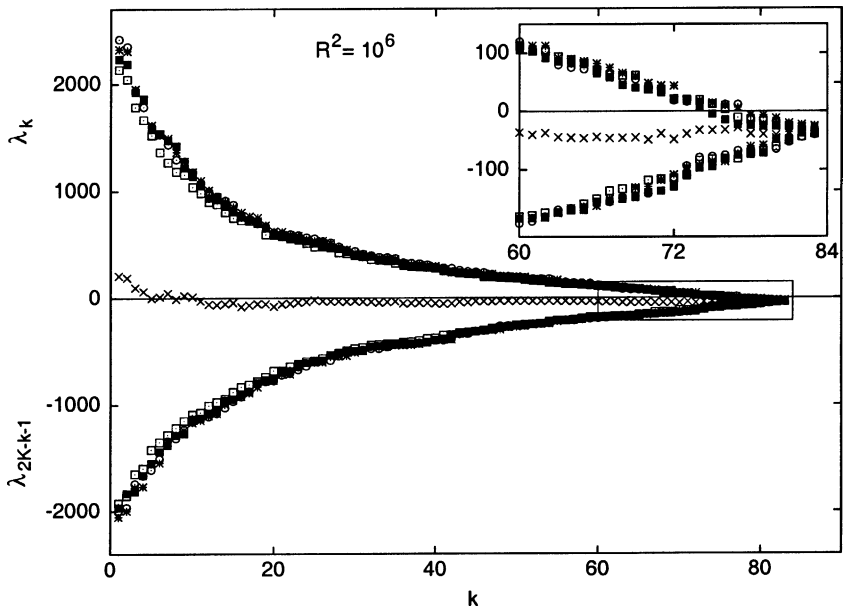

Fig. 2. Lyapunov exponents for one NS run with normal viscosity (⊙) at $N = 7$, $R^2 = 10^6$, and forcing on modes (4, −3), (3, −4). The $2K - 2$ nontrivial exponents are drawn as in Fig. 1. The middle line (×) is the graph of $(\lambda_k + \lambda'_k)/2$. The other symbols refer to the corresponding GNS runs with fixed energy (∗) i.e. $m = 0$, $\ell = 1$, fixed "enstrophy" (□) i.e. $m = 1$, $\ell = 1$, or fixed "palinstrophy" (■) i.e. $m = 2$, $\ell = 1$. The spectra are obtained from runs of different lengths with $T \in [125, 250]$, and with a time step $h \approx 0.0024$, in units of $1/\lambda_{\max}$, $\lambda_{\max}$ being the largest Lyapunov exponent. The overlap of the four spectra (albeit approximate, because of the uncertainties δQ_0, δQ_1 and δQ_2) reflects the validity of the extension of the EC and EC′ to the whole spectrum and to different members of the hierarchy of equations. The error bars (see Section 5) can be identified with the size of the symbols in the large plot. The inset is a magnification of the tip of the spectrum.

Table 1
Equivalence of NS and GNS dynamics ($\ell = 1$ and $m = 0$) for different Reynolds numbers, $N = 3$, and forcing on the modes (0,±2)

R^2	$\delta Q_0/\langle Q_0\rangle_{\rm NS}$	$\Delta\alpha$	ΔQ_1	o(M)/M
800	0.005	0.030	0.053	0.068
1250	0.022	0.018	0.062	0.057
2222	0.002	0.039	0.058	0.077
4444	0.005	0.021	0.093	0.059
5000	0.009	0.008	0.058	0.033

The last column gives the relative difference of the computed sums of the NS and GNS Lyapunov exponents (cf. Eq. (13)). The error bar of the case $R^2 = 1250$ is larger than the others because of computation from a shorter run than those of the other cases.

Table 2
Equivalence for the ED and GED dynamics ($\ell = 0$ and $m = 0$) for different Reynolds numbers, $N = 3$, and forcing on the modes (0,±2)

R^2	$\delta Q_0/\langle Q_0\rangle_{\rm NS}$	$\Delta\alpha$	ΔQ_1	o(M)/M
408	0.004	0.039	0.001	0.060
800	0.001	0.038	0.001	0.067
2222	0.003	0.003	0.002	0.042

For details see legend to Table 1.

If the EC can be extended to such general cases and to cover the Lyapunov spectra, the spectra should overlap (for large R). Considering the fact that the error bars δQ_0, δQ_1, δQ_2 on $\langle Q_0\rangle$, $\langle Q_1\rangle$, $\langle Q_2\rangle$ in these cases were larger than in the cases with $2K = 24$ (the largest being $\delta Q_1 \approx 0.09\langle Q_1\rangle$, our results for $\ell = 1$ and $m = 0, 1, 2$, seem to confirm this property. This is illustrated by Fig. 2 which shows the equivalence, within our numerical accuracy, of the computed Lyapunov spectra of the NS and GNS systems. A similar equivalence was observed in several other cases which we do not describe here for brevity. This reinforces the previous results of [24], and provides a heuristic motivation for the validity of the conjectures EC and EC′.

In Figs. 1 and 2 two exponents for the GNS equation vanish exactly reflecting that Q_0 is a constant of motion and neither expands nor contracts in the direction of the flow. There is a third exponent close to 0 which, however, seems to be numerically distinct from 0. In the NS cases only one exponent is certainly 0 (corresponding to the flow direction) but there are two other exponents which are numerically very close to 0, see also footnote 11.

4. Time reversal symmetry, axiom C and the fluctuation theorem

A fluctuation theorem (FT), [30], for the fluctuations of the phase space contraction rate $\sigma^{\rm GNS}(\boldsymbol{u})$ in our GNS truncated systems can be derived under the assumption that the Chaotic Hypothesis (CH) is consistent with the GNS dynamics at the considered Reynolds number, [14]. The CH can be formulated as follows:

Chaotic Hypothesis (CH). *A chaotic many-particle system or fluid in a stationary state can be regarded, for the purpose of computing macroscopic properties, as a smooth dynamical system with an attracting set on which the system is a smooth transitive Anosov system.*

This means that the attracting set can be considered, *for practical purposes*, to be a connected "smooth surface", on which the dynamics are Anosov (see [12] for a mathematical definition). In other words, one supposes that the attracting set is a smooth surface possibly of dimension lower than that of phase space, thinking that its fractality is not important (here the difference between attracting set and attractor matters: the latter being very often fractal, cf. footnote 2). If the CH is valid for the GNS systems, the FT of [14] follows *provided the attractor is dense in phase space and provided the evolution is time reversible*. The FT imposes strong restrictions, which we illustrate below, on the form of the fluctuations of the contraction of the surface elements on the attracting set (cf. Eq. (9)).

Let $t \mapsto S_t\boldsymbol{u}$ be the time evolution for the initial velocity field $\boldsymbol{u}$ generated by the equations of motion on phase space, and call T the *total* simulation time, which must be adequately longer than the characteristic time θ of the fluctuations of $\sigma^{\rm GNS}$. Assume that relaxation to a statistically stationary state takes place in a time to $t_0 \ll T$ with $t_0 \gg \theta$ where θ is a characteristic time for the evolution, e.g. $\theta = 1/\lambda_{\max}$, and introduce the infinite time average of the phase space contraction rate $\sigma^{\rm GNS}$:

$$\langle\sigma^{\rm GNS}\rangle = \lim_{T\to\infty}\frac{1}{T}\int_0^T \sigma^{\rm GNS}(S_t\boldsymbol{u})\,{\rm d}t = \int \mu({\rm d}\boldsymbol{u})\sigma^{\rm GNS}(S_t\boldsymbol{u}). \tag{14}$$

If T is large, we can subdivide the time interval $[t_0, T]$, into a number of subintervals of length $(\tau + t_d)$, with $\tau \gg \theta$ and t_d a decorrelation time, separating the consecutive evolution segments of length τ. Consider the dimensionless quantities

$$\bar\sigma^{{\rm GNS},\tau}(i) = \frac{1}{\tau\langle\sigma^{\rm GNS}\rangle}\int_{t_0+(i-1)(\tau+t_d)+t_d}^{t_0+i(\tau+t_d)} \sigma^{\rm GNS}(S_t\boldsymbol{u})\,{\rm d}t, \tag{15}$$

with $i = 1, \ldots, (T - t_0)/(\tau + t_d)$ and arrange them in a histogram which allows us to approximate the probability distribution π^τ of the values of $p = \bar\sigma^{{\rm GNS},\tau}$. The total time T is empirically chosen large enough so that larger

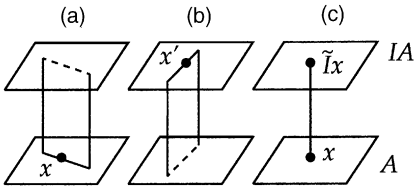

Fig. 3. Illustration of axiom-C systems. The bottom squares represent the attracting set A, while the top squares represent the repelling set IA. The leftmost figure with vertical segments represents a point $x \in A$ with a piece of its stable manifold connecting A to IA. Similarly, the central figure represents a point $x' \in IA$ with a piece of its unstable manifold. The rightmost figure represents the corresponding intersection of the stable manifold of x with the unstable manifold of Ix, which associates a point $\tilde{I}x$ in IA with a point x in A.

simulation times and different initial fields produce differences in the probability distributions that lie within the error bounds over a range of p's which is sufficient to perform meaningful tests.

Within the range of values of p in which the number n of events per histogram bin is statistically meaningful,[9] and for sufficiently large τ, it was observed (cf. [24])that the quantity

$$F(p;\tau) = \frac{1}{\tau\langle\sigma^{\mathrm{GNS}}\rangle}[\log(\pi^\tau(p)) - \log(\pi^\tau(-p))] \tag{16}$$

could be fitted by a function linear in p with slope $c(\tau)$, obtaining:

$$\frac{1}{\tau\langle\sigma^{\mathrm{GNS}}\rangle}[\log(\pi^\tau(p)) - \log(\pi^\tau(-p))] = c(\tau)\,p, \tag{17}$$

within the error bars. If the conditions of the CH and of time reversibility are satisfied, one can check whether or not $c(\tau)$ converges to a limit c_∞, as τ is increased. *If the attractor was really dense in phase space,*[10] *then the validity of the FT would imply that c_∞ exists and, precisely, that $c_\infty = 1$.* In such limiting case we refer to Eq. (17) by calling it the "fluctuation relation" (FR).

However, the attractors of systems with strong dissipation often *are not dense* in phase space. This is the case of the NS equations, in which the attracting sets have a large open complement. In such cases further assumptions are needed before the CH can be used to derive interesting predictions. We shall consider the possibility that there is proportionality between phase space contraction of volume elements *around* the attracting set and contraction of surface elements *on* the attracting set itself (which has dimension lower than that of phase space). This somewhat surprising possibility can be related to (and predicted from) other assumptions which involve geometric and dynamic hypotheses introduced in general in [26] and applied to the GNS equations in [11].

To understand the hypotheses, first note that smoothness of the attracting set and reversibility of the dynamics do not suffice to deduce Eq. (17). Indeed, the image under time reversal of the attracting set A will be a repelling set IA which, if the attractor is not dense in phase space, is disjoint from it, cf. Fig. 3.

Nevertheless, the following may happen and be stable under perturbations of the equations of motion. Consider the stable manifold of the points on the attracting set: part of this manifold will be on the attracting set (which we suppose to be a smooth surface) and another part will stick out, cf. (a) in Fig. 3. Likewise the unstable manifold of the points on the repelling set will be partly on it and partly stick out, cf. (b) in Fig. 3.

It is possible that the parts of the manifolds that stick out cross each other transversally along a manifold that connects the attracting and repelling sets, determining on each of them a single intersection point, cf. the line in (c)

[9] Here, we chose the range with $n \geq 10$ (n being the number of events in a bin), and we weighted the contribution of each bin to the fit as inversely proportional to the associated error bar. In this way, the cases with low statistical relevance (e.g. with $n \approx 10$) have little influence on the computed $c(\tau)$'s and, particularly, on its values extrapolated to large τ.

[10] Hence the whole phase space would be an attracting set.

in Fig. 3. In this way, a correspondence $\tilde{I}$ between attracting set and repelling set is constructed [26]. By construction the map $\tilde{I}$ *commutes* with the time evolution map S_t. The composition I^* of $\tilde{I}$ with the time reversal map I of Eq. (9) leaves the attractor *invariant* and *anticommutes* with time evolution restricted to it, i.e.

$$S_t \cdot I^* = I^* \cdot S_{-t} \quad \text{on the attracting set.}$$

A system with the above geometric properties, introduced and discussed at some length in [26] and in [12,31], is called *Axiom C* system. For such systems, time reversal symmetry can be "spontaneously broken" as a control parameter (R in our case) varies, meaning that the attracting set A becomes smaller than the whole phase space, and distinct from the repelling set IA. However, upon breaking, it spawns a new (lower) symmetry I^* which acts on the attracting set and anticommutes with time evolution. In a sense, in such systems time reversal *cannot be broken* as it is always dynamically regenerated.

In [26,31] this scenario was presented as the simplest possible way in which time reversal symmetry could be spontaneously broken via the splitting of the phase space of a reversible system into an attracting set, a repelling set and a large region in between, as in Fig. 3. *Under this assumption*, the CH holds for the dynamical system obtained by restricting the dynamics to the attracting set. To such system the FT applies, and the fluctuations of the contraction rate *of the area element* of the attracting set obey the FR with an asymptotic slope $c_\infty = 1$.

A further difficulty is that, usually, it is not possible to measure the contraction rate of the surface of the attracting set because this set is a practically inaccessible dynamical object. However, such a measurement is not necessary if one can relate the area contraction on the surface of the attracting set to the total phase space contraction rate which is easily accessible, at least in numerical experiments.

In Figs. 1 and 2 the $2K-2$ nontrivial Lyapunov exponents are arranged in pairs, each consisting of the kth largest exponent and the kth smallest exponent (see [23] for a heuristic theoretical argument motivating this arrangement of our data). We imagine that the pairs with one positive and one negative exponent pertain to the restriction of the evolution to the attracting set.[11] The other pairs, consisting of two negative exponents, would then pertain to the directions of the stable manifold that stick out of the attracting set.

Adopting the above view, we see that in a time T and on the attracting set the phase space contracts by $\sum^*(\Lambda_{k,T} + \Lambda_{2K-1-k,T})$ where $\Lambda_{k,T}$ denotes the "local contraction" exponent of the surface of the attracting set over a time interval T around the phase point occupied by the system at the beginning of the interval. Here, $\sum^*$denotes the summation over the values of k corresponding to pairs of exponents with one positive and one negative exponent. The total contraction of phase space is $\sum_1^K(\Lambda_{k,T} + \Lambda_{2K-1-k,T})$. The two contractions are asymptotic to $T\sum^*(\lambda_k + \lambda_{2K-1-k})$ and to $T\sum_{k=1}^K(\lambda_k + \lambda_{2K-1-k})$, respectively, if λ_k denotes the kth nontrivial Lyapunov exponent. Hence, their ratio tends to

$$c = \frac{\sum^*(\lambda_k + \lambda_{2K-1-k})}{\sum_{k=1}^K(\lambda_k + \lambda_{2K-1-k})} = \lim_{T\to\infty} \frac{\sum^*(\Lambda_{k,T} + \Lambda_{2K-1-k,T})}{\sum_{k=1}^K(\Lambda_k + \Lambda_{2K-1-k})} = \lim_{T\to\infty} C(T). \tag{18}$$

If the ratio $C(T)$ is constant over the typical time scales over which we observe the fluctuations of the phase space contraction, there is proportionality between the phase space contraction and the area contraction on the surface, and the proportionality constant is precisely c (which implies a weaker property than the one envisaged in [23]: the latter in fact seems too strong and not applicable to the present case). We have tested whether this is the case, by taking as time scale $1/\lambda_{\max}$, the inverse of the largest Lyapunov exponent. The result is that, after a short transient,

[11] By the axiom C, i.e. by the consequent existence of a time reversal symmetry on the attracting set, we know that on such set half of the exponents is positive and half is negative, once the vanishing exponent associated with the flow direction has been discarded together with the other vanishing exponent associated with the conserved quantity (energy, or enstrophy or any of the global quadratic quantities Q_m, depending on the model). Arranging the remaining $2K-2$ exponents in decreasing order: $\lambda_1 \geq \lambda_2 \geq \cdots \geq \lambda_{2k-2}$, one can form the pairs (λ_k, λ'_k) of Figs. 1 and 2.

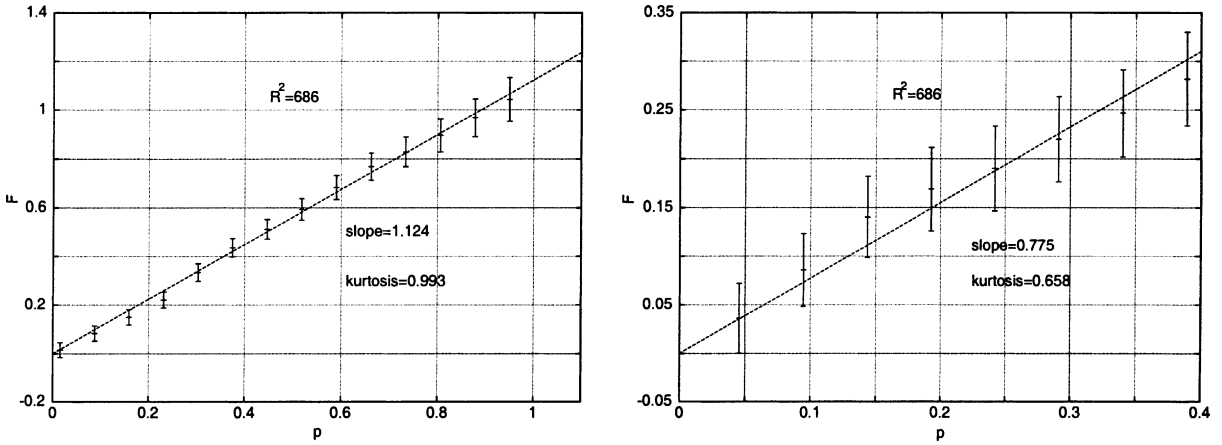

Fig. 4. Computed values of $F(p;\tau)$, Eq. (16), for a GNS system with fixed energy ($\ell = 1$, $m = 0$) and $R^2 = 686$. The straight lines interpolate the data, and the error bars represent the statistical errors. The left panel has $\tau \approx 1.2$, while the right panel has $\tau \approx 2.5$, in $1/\lambda_{\max}$ units. In order to obtain the fit in Fig. 5 we repeated similar measurements for various values of τ. Data refer to a 24-real modes truncation ($2K = 24$). The data for $p < 0$ can be inferred from the symmetry $p \leftrightarrow -p$. The kurtosis of π^τ is defined by $\langle(p-1)^4\rangle/\langle(p-1)^2\rangle^2$, and equals 3 if π^τ is Gaussian.

the quantity $C(T)$ is indeed practically constant (with fluctuation amplitudes of a few percent of its average value) while the phase space contraction fluctuates with *much larger* amplitudes. This is also reflected, for instance, in the variances of the histograms of $C(T)$ with short T's for the cases we checked, which are more than one order of magnitude smaller than the variances of the corresponding histograms of the phase space contraction. Therefore, the FR with slope 1 for the (not directly accessible) surface contraction on the attracting set will imply a FR for the *total* (measurable) phase space contraction with a slope c given by Eq. (18).

If in Eq. (16) we use the histograms for π^τ obtained as outlined above, the result is well fitted by the linear law (17). This is the case starting from τ's comparable to $1/\lambda_{\max}$, and remains valid throughout the range of τ's that we can consider. In this range, the values of $c(\tau)$ can be computed through a least square fit and, as suggested by the CH, the results can be interpolated by a function like

$$c_\infty + \frac{A}{\tau}, \tag{19}$$

where c_∞ is the asymptotic slope and A is a constant: in fact, in Anosov systems the limit of $\tau^{-1}\log\pi^\tau(p)$ is reached with errors of order τ^{-1}, as $\tau \to \infty$ [14,30]. In all cases we considered, such an interpolation fits our data well. Figs. 4 and 5 illustrate that the above statements are valid even in the cases with small R^2. The reason for the smallness of the τ's that we can consider can be understood by looking at Fig. 4 where, by comparing the graph on the left panel (smaller τ) with the one on the right panel (larger τ), we see that the range of p's over which Eq. (16) can be assessed rapidly decreases with τ. This is due to the decrease of the frequency of the negative fluctuations of $\bar\sigma^{\mathrm{GNS},\tau}$, which rapidly becomes practically zero as τ grows.

Nevertheless, the interpolation by $c_\infty + A/\tau$, where the c_∞ and A are obtained from a least square fit, looks convincing within our range of τ's and we therefore investigate the consequences of assuming that it remains valid beyond this range. In this case, one can compare the values of c_∞ with those of c obtained from Eq. (18). The results are reported in Tables 3 and 4. One realizes that, within the accuracy of our numerical results, discussed more in detail in the next section, there is agreement between the predictions of [23] for c and our values for c_∞. Of course, this is only a consistency check of the axiom C hypothesis which, as mentioned above, can only be indirectly tested in our cases.

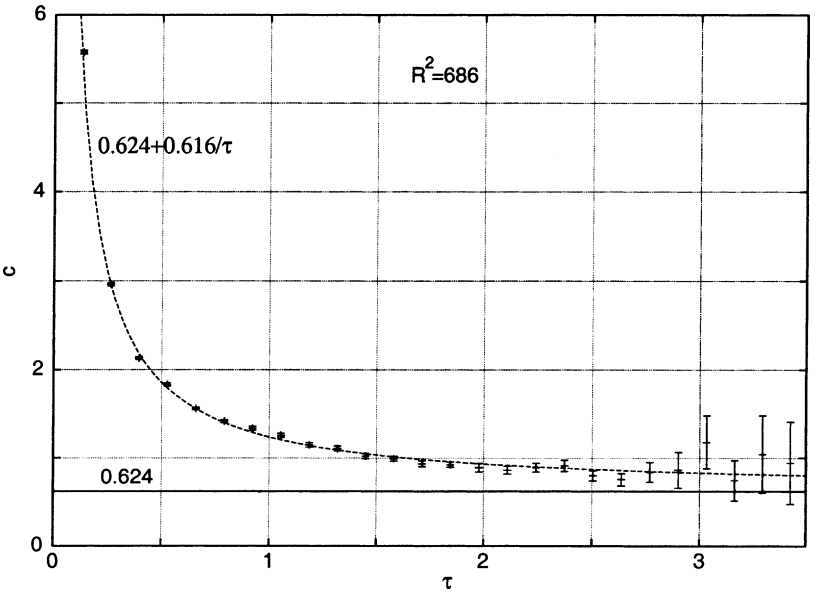

Fig. 5. The value $c(\tau)$ for the GNS run with fixed energy ($\ell = 1, m = 0$), $R^2 = 686$. The times τ, in the horizontal axis are given in $1/\lambda_{\max}$ units. Data refer to a 24-real modes truncation ($2K = 24$) and to values of τ to which already corresponds a linear graph of $F(p; \tau)$. The datum with smallest τ has not been used in constructing the fit (but it matches it, nevertheless).

Table 3
Properties of the GNS dynamics with fixed energy ($\ell = 1, m = 0$)

R^2	c	c_∞	KY	D_P
556	0.534	$0.535 \pm 0\,010$	0.734	0.565 ($n_- = 5$)
638	0.436	0.421 ± 0.020	0.610	0.478 ($n_- = 6$)
686	0.630	0.624 ± 0.013	0.848	0.652 ($n_- = 4$)
800	0.639	0.614 ± 0.025	0.830	0.652 ($n_- = 4$)
1250	0.639	0.699 ± 0.015	0.845	0.652 ($n_- = 4$)
2222	0.834	0.713 ± 0.010	0.914	0.826 ($n_- = 2$)
5000	0.842	0.840 ± 0.014	0.939	0.826 ($n_- = 2$)

The value of c is obtained from Eq. (18) using the measured Lyapunov exponents. The value c_∞ is obtained by extrapolation of the data as in Fig. 5. The column labeled by KY, gives the Kaplan–Yorke dimension computed from our measured Lyapunov exponents. The column labeled by D_P is the ratio $(2K - 1 - 2n)/(2K - 1)$ where n_- is the number of pairs with two negative Lyapunov exponents. Data refer to a 24-real modes truncation ($2K - 1 = 23$). Our estimate of n_-, given in brackets in the column of D_P, affects the calculations of both c and D_P. The simulations of the case $R^2 = 1250$ are shorter than the other simulations.

Table 4
Properties of the GED dynamics with fixed energy ($\ell = 0, m = 0$)

R^2	c	c_∞	KY	D_P
408	0.911	0.823 ± 0.010	0.943	0.913 ($n_- = 1$)
556	0.813	0.815 ± 0.011	0.957	0.826 ($n_- = 2$)
800	0.910	0.903 ± 0.008	0.983	0.913 ($n_- = 1$)

The meaning of the columns is the same as in Table 3. Data refer to a 24-real modes truncation ($2K - 1 = 23$).

We also remark that the axiom C hypothesis leads to a simple expression for the dimension of the attracting set, according to which the ratio between the dimension of the attracting surface (on which the attractor is dense) and the dimension of the phase space ($2K-1$ in our cases because of the existence of the conserved quantity Q_0) is the ratio $D_P = (2K-1-2n_-)/(2K-1)$, where n_- is the number of pairs with two negative Lyapunov exponents. Obviously, the fractal dimension of the attractor cannot be larger than the dimension of the attracting surface. Therefore, under our assumptions on the nature of the attracting set, if the Kaplan–Yorke dimension is a measure of the fractal dimension of the attractor, its value divided by $2K-1$ should be $\leq D_P$. It is therefore of some interest to check whether this holds in our case or not.

In most cases (e.g. in the cases of Fig. 1) there are three exponents very close to 0 and they are affected by a large relative error (see comments in Section 5). We interpret as 0 the two of smallest absolute value (as we know that two exponents necessarily vanish). Although the signs of the second and third smallest exponents are stable with the length of our simulations, some uncertainty remains, at times, on which of the two approximates a zero exponent, and which approximates a finite exponent. For this reason, the values n_- reported in brackets in Tables 3 and 4 are uncertain by 1, and this implies an uncertainty also on the calculations of c and D_P (cf. point 3 of Section 6).

Table 3 shows that in our system the axiom C prediction and the KY value do not seem really compatible. The comparison of the dimensions and its consequences has been suggested by F. Bonetto. The incompatibility between the axiom C and the KY methods for determining the fractal dimension of an attractor seems to be quite general and to apply to rather different kinds of chaotic motions.

The same questions addressed here have been investigated in the case of the GED equations, obtaining the results reported in Table 4.

It should be noted that the a priori pairing assumption which, together with axiom C, allowed us to interpret and organize our data, does not have firm theoretical grounds other than the discussion in [11]. Therefore, the above analysis is highly conjectural and finds its main justification in its capability to fit the data.

5. Technical comments on the simulations: accuracy

The calculations summarized by Figs. 1, 4 and 5, and by Tables 1–4, all refer to cases with rather small R and N compared to the cases studied in [24]. Small R is needed to obtain values of c_∞ sufficiently small to be distinguished clearly from 1, while small N is needed to compute with reasonable accuracy the Lyapunov spectra. The actual values R and N that we chose constitute a compromise, but the result is that the frequency of the negative fluctuations, needed for a test of the fluctuation formula, is quite low, and very rapidly it becomes negligible for growing τ's, even in long simulations. Given our present computer facilities, our standard simulation was of order of 10^8 time steps, with sizes DT of order between 10^{-6} and 10^{-4}, corresponding to times T of order between 10^3 and 10^5 in $1/\lambda_{\max}$ time units.

Such T's suffice for calculations of the average of quantities like the Q_m's, and to build with some accuracy the histograms of the fluctuations of $\bar\sigma^{\mathrm{GNS},\tau}$ for relatively small τ's. The accuracy is reflected by the error bars placed on the computed quantities, like in Figs. 4 and 5, which cover the range of τ's beyond which the negative fluctuations are too rare to have any statistical significance (cf. footnote 8). These bars represent the statistical errors, obtained from the error bar on the histogram for π^τ, i.e. $\pm\sqrt{n}$ on a bin, if n is the number of counts in that bin.

The times T are also sufficient for an accurate evaluation of the largest Lyapunov exponents. Indeed, out of 24, the largest (in absolute value) 20 exponents have an uncertainty ranging from 25% down to 0.06% of the computed value, for the largest one. The uncertainty on the remaining 4 (smallest) exponents at times exceeds 100% of the computed value. The uncertainty on one exponent has been evaluated as the amplitude of the largest fluctuation of the computed value of that exponent in the second half of a simulation of length T. In all cases, the error bars do not

exceed the symbols size, if drawn in figures such as Fig. 1. Nevertheless, at times, it is not obvious which two, of the three smallest exponents, vanish and which does not. This makes n_- uncertain by one unit. In particular, in the GNS case with $R^2 = 2222$ and in the GED case with $R^2 = 408$, n_- could have been taken to be 3 and 2, respectively, rather than 2 and 1 as reported in Tables 3 and 4. In fact, the third and the second smallest exponents are both quite small and close in absolute value, but the third smallest is positive while the second smallest is negative. Therefore, considering zero the third smallest exponent, rather than the second, makes n_- grow by 1.

The slopes $c(\tau)$, from which the values c_∞ of Tables 3 and 4 have been extrapolated, were computed by fitting our data to Eq. (17) and by using our histograms of $\bar\sigma^{\mathrm{GNS},\tau}$ for π^τ. The limiting slopes c_∞ and its error bar reported in Tables 3 and 4 have been computed by a least square fit the function $c_\infty + A/\tau$ to the $c(\tau)$'s.

6. Concluding remarks

1. The results on the equivalence between NS and GNS dynamics obtained in [24] have been strengthened through the analysis of the Lyapunov spectra of NS and GNS systems, albeit at very low spectral resolution. Similar results were obtained for spectral resolutions with up to 190 modes.
2. The paper [32] studies a similar equivalence conjecture for the shell model. The authors of this paper observe that "the dynamical ensemble equivalence seems to be satisfied at least for the typical observables measurable in turbulent flows" (cf. [32], p. 31), however the statistics of their shell model and of their corresponding constrained equation are not fully equivalent. Hence, one may expect that also the Lyapunov spectra of the two models differ. The shell model permits us to investigate the behavior of systems with many more "shells" than we can for the NS and GNS systems. Although the shell model is quite different from the few modes models that we study this might mean that if our experiment was pushed to much higher truncations it would also show differences from the behavior expected on the basis of the equivalence conjectures. Unfortunately, with the present computer facilities we are not able to study this question.
3. The results of [24] on the validity of the FR for the GNS dynamics have been strengthened. Unfortunately, the relatively high dissipation of the systems considered here did not allow us to study the fluctuations of $\bar\sigma^{\mathrm{GNS},\tau}$, with $\tau \gg 1/\lambda^+_{\max}$, as desired, due to lack of appreciably frequent negative fluctuations at such τ's. Nevertheless, our data are well fitted by $c_\infty + A/\tau$, in the whole ranges of τ we considered, in accordance with the validity of the CH.
4. The Lyapunov spectra have been used to compute the values c of Eq. (18) reported in Tables 3 and 4. These values equal the corresponding quantities c_∞ in agreement with the axiom-C hypothesis, except for the GNS case with $R^2 = 2222$ and for the GED case with $R^2 = 408$. The uncertainty on c looks more pronounced than the uncertainty on c_∞, because of the uncertainty on the number of positive Lyapunov exponents arising from the fact that often one of them is too close to 0.[12] The effect of this uncertainty on c is about 9%, since it affects the number of pairs appearing in the numerator of Eq. (18) by 1, and the contributions of the different pairs do not fluctuate much around their average value. In particular, in the GNS case with $R^2 = 2222$ and in the GED case with $R^2 = 408$, taking $n_- = 3$ and $n_- = 2$ respectively, leads to a close agreement between c and c_∞ also in these two cases.
5. Our codes, considered as dynamical systems in their own, appear like axiom C systems, within the time scales of our simulations. Whether this property can be inferred to hold for the dynamics of real fluids is not clear, because of the low spectral resolution we have used.

[12] Two exponents have to vanish: the one corresponding to the conserved quantity Q_m, and the one corresponding to the direction of the flow. However there are other exponents very close to zero, and one faces, therefore, the difficult task of distinguishing numerically the small (positive or negative) exponents from the vanishing ones.

6. Global fluctuations of macroscopic systems can hardly be observed, although the experiments of [15,16] attempt at studying precisely this kind of fluctuations. However, as argued in the Appendix, the (observable) local fluctuations seem to obey laws similar to those of the global fluctuations discussed here.
7. The extrapolation hypothesis Eq. (19) leads to a slope c_∞ which has been fitted to a value <1. If confirmed by further experiments, this implies that the stochastic fluctuation theorems which lead to $c_\infty = 1$, such as those recently proposed in [33], would require extra ideas to be adapted to the description of the fluctuations of our deterministic dynamical systems.

Acknowledgements

We are grateful to S. Ciliberto and C.P. Dettmann for highly stimulating discussions. LR gratefully acknowledges partial support from GNFM. We are particularly indebted to F. Bonetto for suggesting several improvements and for clarifying the meaning of the pairing rule, which resulted in the correction of an error in the manuscript. GG and LR thank B. Dorfman, P Gaspard, R. Klages, H. van Beijeren and the Max Planck Institute for Physics of Complex Systems, Dresden, for their generous and warm hospitality during the conference "Microscopic Chaos and Transport in Many-Particle Systems". The project and the data interpretation is joint work of the three authors. The software construction and the execution of the numerical experiments is due to L.R and E.S.

Appendix A. Remarks on local fluctuations and on spatio-temporal chaos

Recently, local versions of the FT have been considered to overcome the problem that the large global fluctuations which are the object of the original FT cannot be observed in real macroscopic systems. One possible approach has been outlined in [34], where a fluctuation relation similar to (17) has been derived for the fluctuations of local quantities, in an infinite chain of weakly interacting chaotic maps, which is a paradigmatic system exhibiting spatio-temporal chaos. In particular, let V_0 be a finite region of the chain centered at the origin, $T_0 > 0$ be a time interval, and define η_+ and p as

$$\eta_+ = \lim_{V_0, T_0 \to \infty} \frac{1}{|V_0| T_0} \sum_{j=0}^{T_0-1} \eta_{V_0}(S^j x), \qquad p = \frac{1}{\eta_+ |V|} \sum_{j=-T_0/2}^{T_0/2} \eta_{V_0}(S^j x), \tag{A.1}$$

where $V = V_0 \times T_0$, and $\eta_{V_0}(x)$ is a properly chosen quantity which in [34] is called the *entropy production rate in* V_0 and is identified with the phase space contraction rate in V_0. The following relation was obtained for the steady-state probability distribution of p:

$$\pi_V(p) = e^{\zeta(p)|V| + O(|\partial V|)}, \tag{A.2}$$

with

$$\frac{\zeta(p) - \zeta(-p)}{p\eta_+} = 1 \quad \text{and} \quad p| < p^*,$$

where $|\delta V|$ is the size of the boundary of V, $p^* \geq 1$ and ζ is analytic in p. This is perfectly analogous to the original FT, except for the boundary term $|\delta V|$ whose influence should diminish with growing V.

The question of the validity of relations analogous to Eqs. (A.1) and (A.2) in 2-dimensional fluids is beyond the scope of the present paper. Nevertheless, it seems worthwhile to report our encouraging preliminary results on the validity of a local fluctuation relation for the NS dynamics. In fact, these results make plausible a linear relation with slopes smaller than 1, and indicate that in the NS case, in which dissipation occurs uniformly throughout the

system, the local fluctuations may obey laws very similar to those obeyed by the global fluctuations considered in the previous sections. The interest lies in the possibility that, in agreement with the EC, the local fluctuations can be observed also in the NS dynamics, despite their irreversibility.

The first study of a local fluctuation relation to obtain the value of c_∞ is in [35], and the problem has raised many discussions since.

Let us consider the NS equation on a periodic cell of side 2π, and let $V_0 = [-L/2, L/2] \times [-L/2, L/2]$ be a box with side $L \le 2\pi$. We define the power dissipated in V_0 by the forcing field $\boldsymbol{f}$ at time t as

$$\hat{p}_L(t) = \int \boldsymbol{f}(x) \cdot \boldsymbol{u}(\boldsymbol{x}, t) \chi_{V_0}(\boldsymbol{x}) \, \mathrm{d}\boldsymbol{x}, \tag{A.3}$$

where χ_{V_0} is the characteristic function of V_0 which, in spectral form, is: $\chi_{V_0}(\boldsymbol{x}) = \sum_{\boldsymbol{k}} \chi_{\boldsymbol{k}}(L) \, \mathrm{e}^{\mathrm{i}\boldsymbol{k}\cdot\boldsymbol{x}}$. Defining local vorticity, local palinstrophy and α_L, respectively, as

$$\begin{aligned} Q_{1,L}(t) &= \int \omega^2(\boldsymbol{x}, t) \chi_{V_0}(\boldsymbol{x}) \, \mathrm{d}\boldsymbol{x}, \\ Q_{2,L}(t) &= \int (\nabla\omega)^2(\boldsymbol{x}, t) \chi_{V_0}(\boldsymbol{x}) \, \mathrm{d}\boldsymbol{x}, \\ \alpha_L(t) &= \frac{\hat{p}_L(t)}{Q_{1,L}(t)}, \end{aligned} \tag{A.4}$$

with $\omega = \nabla \times \boldsymbol{u}$, we propose to take $\eta_{V_0}(\boldsymbol{u})$ as proportional to the work per unit time performed by the external force within the region V_0 divided by the corresponding local vorticity, i.e. we propose to take $\eta_{V_0}(\boldsymbol{u})$ proportional to α_L This is suggested by the facts that such a quantity has a physical meaning, and that the phase space contraction rate can in many systems be identified with the entropy production rate. In fact, $Q_{1,L}$ can be called a "local temperature" being a quantity whose value measures the variations of the velocity field around its average. A possible alternative definition is a local version of Eq. (10), like (for instance)

$$\hat{\sigma}_L = 2 \left(\left(\frac{L}{2\pi} \right)^2 \sum_{|k_i| \le N} |k_i|^2 - \frac{Q_{2,L}}{Q_{1,L}} \right) \cdot \alpha_L + \frac{\int \nabla f \, \nabla\omega \, \chi_{V_0} \, \mathrm{d}\boldsymbol{x}}{Q_{1,L}} \tag{A.5}$$

(the summation runs over the independent modes). However, several other local versions of Eq. (10) could be defined: e.g. the last integral could be replaced by $\int \nabla^2 f \omega \, \chi_{V_0} \, \mathrm{d}\boldsymbol{x}$ or by $\int f \, \nabla^2\omega \, \chi_{V_0} \, \mathrm{d}\boldsymbol{x}$.

Since we approximate the various quantities introduced above by means of truncated Fourier expansions, L can only take the values $l\pi/(N-1)$ with $l = 1, \ldots, 2(N-1)$.

Studying the behavior of $\sigma_L = \hat{\sigma}_L / \langle \hat{\sigma}_L \rangle$, $\langle \hat{\sigma}_L \rangle$ being the infinite time average of $\hat{\sigma}_L$, one realizes that $\hat{\sigma}_L$ is essentially proportional to α_L, with proportionality constant equal to the ratio $\langle \hat{\sigma}_L \rangle / \langle \alpha_L \rangle$, because the sum in (A.5) dominates over the other terms already at moderately large L. In particular, we performed a number of simulations with $N = 7$ (i.e. 84 complex Fourier modes) and $R^2 = 2048$, and we found that $\hat{\alpha}_L / \langle \hat{\alpha}_L \rangle$ and $\hat{\sigma}_L / \langle \hat{\sigma}_L \rangle$ are practically indistinguishable from each other for $L \ge 5\pi/6$. The statistics of the fluctuations of $\hat{\sigma}_L$ was built from a run of 1.36×10^8 time steps, corresponding to 2.4×10^4 in $1/\lambda_{\max}$ time units.

As in the case of global fluctuations (cf. Fig. 4, and [24]), we found that the PDFs of the fluctuations of the average of σ_L over times T_0 are not Gaussian (cf. Table A.1, and Fig. 7), and furthermore that the quantity

$$F(p; V) = \frac{1}{T_0 \langle \hat{\sigma}_L \rangle} \log \frac{\pi_V(p)}{\pi_V(-p)} \quad \text{with} \quad p = \frac{1}{T_0 \langle \hat{\sigma}_L \rangle} \int_t^{t+T_0} \hat{\sigma}_L(s) \, \mathrm{d}s \tag{A.6}$$

is not linear in p at small V (i.e. small L, or small T_0), but it appears to be better and better approximated by a straight line of slope $c(V)$ as V grows. Moreover, the slopes of the linear fits of the data appear to converge to values c_L for $T_0 \to \infty$. Fig. 6 illustrates the latter convergence at fixed box size L and growing T_0, showing that a linear fit of the

Table A.1
Kurtosis of π_V for the cases of Fig. 6

T_0	$L = \pi$	$L = 5\pi/3$
0.58	2.002	1.249
1.75	1.065	1.476
5.27	1.532	1.120
7.81	1.215	1.448
10.74	0.928	1.066

These values show that such PDFs are not Gaussian.

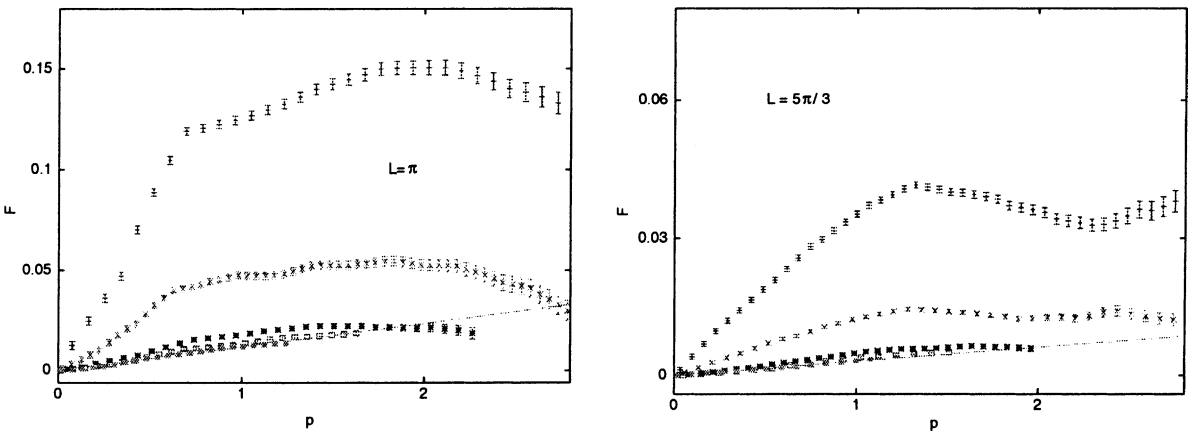

Fig. 6. Numerically computed values of $F(p; V)$, and corresponding error bars, for $L = \pi$ (left) and $L = 5\pi/3$ (right). In each panel we have five curves, corresponding to $T_0 \approx 0.58, 1.75, 5.27, 7.81, 10.74$ (in $1/\lambda_{\max}$ units), ordered clockwise with growing T_0. Only three curves are clearly distinguishable because the three of highest T_0 practically overlap in their range of coexistence, which shrinks with increasing T_0.

data becomes acceptable at sufficiently large T_0, and suggesting that the slope of the fitting line may converge to a limit value.

Fig. 7 shows that the same holds if T_0 is fixed and L grows, indicating that the nonlinear tails of F, may possibly be ascribed to non-negligible boundary contributions, which become less important at larger L. In fact, we notice

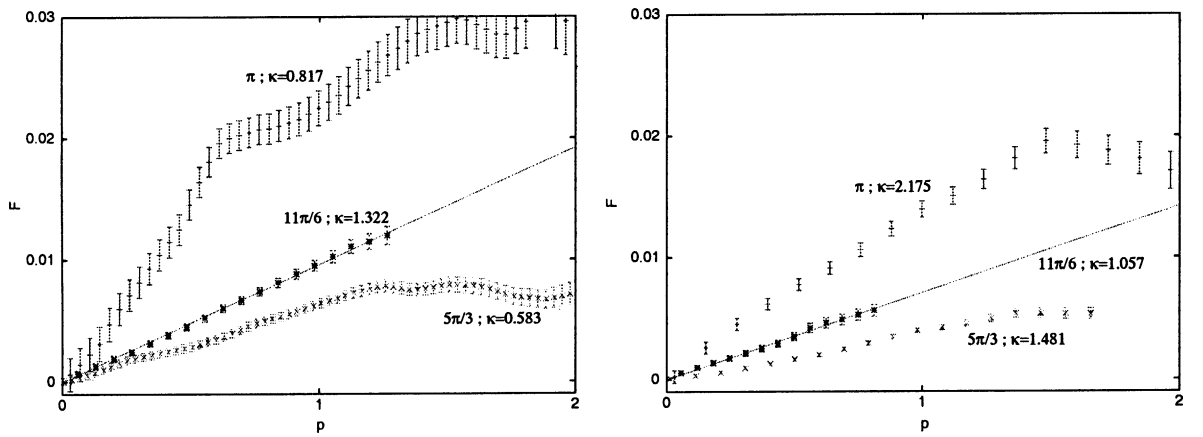

Fig. 7. Values of $F(p; V)$, and corresponding error bars, for $T_0 \approx 3.7$ (left) and $T_0 \approx 7.0$ (right) in $1/\lambda_{\max}$ units. In each panel we have three curves, corresponding to $L = \pi, 5\pi/3, 11\pi/6$, and the values κ of represent the kurtosis of the corresponding PDFs.

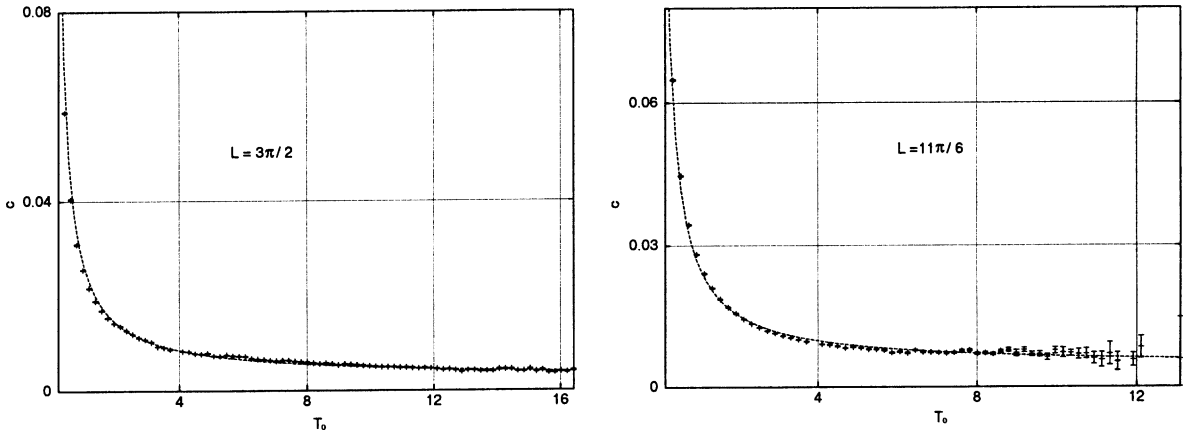

Fig. 8. Slopes $c(V)$ for fixed V_0 as a function of T_0 (in $1/\lambda_{\max}$ time units). The left panel has $L = 3\pi/2$ and the data are interpolated by $c = 0.0025 + 0.024/T_0$. The right panel has $11\pi/6$ and the data are interpolated by $c = 0.0043 + 0.022/T_0$.

that, for any V, $F(p; V)$ is linear in a given neighborhood I_0 of $p = 0$, even if strong nonlinearities characterize F outside I_0. As V grows, it seems that the linear region persists, although it changes slope, while the nonlinear tails of F gradually disappear. Therefore, our data for F justify a test of the local fluctuation formula (A.2), in analogy with the theory of [34]. The result is summarized in Fig. 8, where the slopes c of the linear fits our data, and their variation with growing τ are portrayed. There, we observe that our results for the local fluctuations are consistent with the EC and EC′, and with linear relations with limit slopes smaller than 1. Slopes < 1 have also been previously found for local fluctuations in rather different systems, [35].

We conclude by remarking that

(a) our definition of the local phase space contraction rate (A.5) equals (up to a scaling factor) the physically measurable quantity α_L for sufficiently large L, which in our case amounts to $L = l\pi/6$ for $l = 5, 6, \ldots, 12$;
(b) the fluctuations of the local quantities $\hat{p}_L$ and $\hat{p}_L/Q_{0,L}$, with $Q_{0,L} = \int \boldsymbol{u}^2(\boldsymbol{x}, t)\chi_{V_0}(\boldsymbol{x})\,\mathrm{d}\boldsymbol{x}$, behave in a perfectly analogous way as the fluctuations of $\hat{\sigma}_L$. The latter remark is important because in the experimental work of [16] the quantity which is measured to attempt a check of the FR is essentially the global work $\hat{p}_L$, $L = 2\pi$, done by the external forces per unit time, rather than the same quantity divided by an effective temperature;
(c) the fluctuation laws tested in Appendix A concern the (*irreversible and constant friction*) NS equation, and not the (*reversible and fluctuating friction*) GNS dynamics. This is consistent with the validity of the EC and EC′.

References

[1] R. Ruelle, What are the measures describing turbulence?, Prog. Theor. Phys. 64 (Suppl.) (1978) 339.
[2] T. Bohr, M.H. Jensen, G. Paladin, A. Vulpiani. Dynamical Systems Approach to Turbulence. Nonlinear Science Series, No. 7, Cambridge University Press, Cambridge, 1998.
[3] R. Grappin, J. Léorat, Lyapunov exponents and the dimension of periodic incompressible Navier–Stokes flows: numerical measurements, J. Fluid Mech. 222 (1991) 61–94.
[4] J. Lee, Chaos and direct numerical simulation in turbulence, Theor. Comput. Fluid Dyn. 7 (1995) 363–395.
[5] J.P. Eckmann, D. Ruelle, Ergodic theory of chaos and strange attractors, Rev. Modern Phys. 57 (1981) 617–656.
[6] E. Lieb, On characteristic exponents in turbulence, Commun. Math. Phys. 92 (1984) 473–480.
[7] D. Ruelle, Large volume limit of the distribution of characteristic exponents in turbulence, Commun. Math. Phys. 87 (1982) 287–302.
[8] M. Yamada, K. Ohkitani, Lyapunov spectrum of a model of two-dimensional turbulence, Phys. Rev. Lett. 60 (11) (1988) 983–986.

[9] M. Yamada, K. Ohkitani, Asymptotic formulas for the Lyapunov spectrum of fully developed shell model turbulence, Phys. Rev. E 57 (6) (1998) R6527–6260.
[10] R. Benzi, G. Paladin, G. Parisi, A. Vulpiani, Multifractal and intermittancy in turbulence, in: C. Basdevant, R. Benzi, S. Ciliberto, (Eds.), Turbulence in Spatially Extended Systems, Nova Science, New York, 1993.
[11] G. Gallavotti, Equivalence of dynamical ensembles and Navier-Stokes equations, Phys. Lett. A 223 (1996) 91.
[12] G. Gallavotti, Foundations of Fluid Mechanics. Texts and Monographs in Physics. Springer-Verlag, Berlin, 2002.
[13] G. Gallavotti, Statistical Mechanics: A Short Treatise. Springer-Verlag, Berlin, 1999.
[14] G. Gallavotti, E.G.D. Cohen, Dynamical ensembles in stationary states, J. Statist. Phys. 80 (5/6) (1995) 931.
[15] S. Ciliberto, C. Laroche, An experimental test of the Gallavotti-Cohen fluctuation theorem, J. de Physique IV 8 (6) (1998) 215.
[16] W.I. Goldburg, Y.Y. Goldschmidt, H. Kellay, Fluctuation and dissipation in liquid crystal electroconvect ion, preprint, 2001.
[17] D.J. Evans, D.J. Searles, Equilibrium microstates which generate second law violating steady states, Phys. Rev. E 50 (1994) 1645.
[18] E.G.D. Cohen, G. Gallavotti, Note on two theorems in nonequilibrium statistical mechanics, J. Statist. Phys. 96 (5) (1999) 1343–1349.
[19] M. Germano, A proposal for a redefinition of the turbulent stresses in the filtered Navier–Stokes equations, Phys. Fluids 5 (1986) 1282–1284.
[20] C. Meneveau, J. Katz, Scale-invariance and turbulence models for large eddy simulation, Ann. Rev. Fluid Mech. 32 (2000) 1–32.
[21] Z.S. She, E. Jackson, Constrained Euler system for Navier Stokes turbulence, Phys. Rev. Lett. 70 (9) (1993) 1255–1258.
[22] E. Léveque, C.R. Koudella, Finite-mode spectral model of homogeneous and isotropic Navier-Stokes turbulence: a rapidly depleted energy cascade, Phys. Rev. Lett. 86 (18) (2001) 4033–4036.
[23] G. Gallavotti, Dynamical ensemble equivalence in fluid mechanics, Physica D 105 (1997) 163.
[24] L. Rondoni, E. Segre, Fluctuations in two-dimensional reversibly damped turbulence, Nonlinearity 12 (6) (1999) 1471–1487.
[25] Ch. Dellago, W. Hoover, H. Posch, Lyapunov instability in a system of hard disks in equilibrium and nonequilibrium steady states, Phys. Rev. E 53 (1996) 1485.
[26] F. Bonetto, G. Gallavotti, Reversibility, coarse graining and the chaoticity principle, Commun. Math. Phys. 189 (1997) 263–276.
[27] C. Giberti, L. Rondoni, C. Vernia, Coexistence of chaotic and non-chaotic states in the two-dimensional Gauss–Navier–Stokes dynamics, Physica D 187 (2004) 358–369.
[28] G. Benettin, L. Galgani, J.M. Giorgilli, A. Strelcyn, Lyapunov characteristic exponents for smooth dynamical systems and for hamiltonian systems; a method for computing all of them. part 1: Theory, part 2: Applications. MEC 15 9-20 and 21-30, 1980.
[29] C.P. Dettmann, G.P. Morriss, Proof of Lyapunov exponent pairing for systems at constant kinetic energy, Phys. Rev. E 53 (1996) R5541.
[30] G. Gallavotti, E.G.D. Cohen, Dynamical ensembles in nonequilibrium statistical mechanics, Phys. Rev. Lett. 74 (1995) 2694.
[31] G. Gallavotti, Breakdown and regeneration of time reversal symmetry in nonequilibrium statistical mechanics, Physica D 112 (1998) 250–257.
[32] L. Biferale, D. Pierotti, A. Vulpiani, Time-reversible dynamical systems for turbulence, J. Phys. A 31 (1998) 21.
[33] C. Maes, The fluctuation theorem as a Gibbs property, J. Statist. Phys. 95 (1999) 367–392.
[34] G. Gallavotti, A local fluctuation theorem, J. Phys. A 263 (1999) 39–50.
[35] F. Bonetto, J.L. Lebowitz, Thermodynamic entropy production fluctuation in a two dimensional shear flow model, Phys. Rev. E 64 (2001) 56129–56138.